

# On the Electron Agyrotropy during Rapid Asymmetric Magnetic Island Coalescence in Presence of a Guide Field

E. Cazzola<sup>\*1</sup>, M. E. Innocenti<sup>1</sup>, M. V. Goldman<sup>2</sup>, D. L. Newman<sup>2</sup>, D.S. Markidis<sup>3</sup>, and G. Lapenta<sup>1</sup>

<sup>1</sup>Department of Mathematics, KULeuven University, Celestijnenlaan 200B, Leuven, 3001, Belgium.

<sup>2</sup>Center for Integrated Plasma Studies, University of Colorado Boulder, Boulder, Colorado, USA.

<sup>3</sup>PDC Center for high Performance Computing, KTH Royal Institute of Technology, Teknikringen 14, 10044 Stockholm, Sweden.

August 3, 2016

## Abstract

We present an analysis of the properties of the electron velocity distribution during island coalescence in asymmetric reconnection with and without guide field. In a previous study, three main domains were identified, in the case without guide field, as X-, D- and M-regions featuring different reconnection evolutions (Cazzola *et al.*, 2015). These regions are also identified here in the case with guide field. We study the departure from isotropic and gyrotropic behavior by means of different robust detection algorithms proposed in the literature. While in the case without guide field these metrics show an overall agreement, when the guide field is present a discrepancy in the agyrotropy within some relevant regions is observed, such as at the separatrices and inside magnetic islands. Moreover, in light of the new observations from the Multiscale MagnetoSpheric mission, an analysis of the electron velocity phase-

space in these domains is presented.

## 1 Introduction

Magnetic reconnection is a highly multi-scale physical process occurring in plasmas when magnetic field lines with opposite polarity come in contact. The process releases a large amount of the stored magnetic energy after a complete restructuring of the magnetic field topology. This effect makes reconnection one of the most important sources of accelerated particles in space. However, magnetic reconnection alone cannot explain the high energy particles measured in some regions in space, and other accelerating processes have to be taken into account alongside reconnection. One of the most solid explanation involves multiple acceleration mechanisms during the formation, growth and coalescence of magnetic islands (Drake *et al.*, 2006; Oka *et al.*, 2010). While the effects of island coalesce in symmetric reconnection have been sufficiently

---

<sup>\*</sup>emanuele.cazzola@wis.kuleuven.be

studied over the decades, the same process in asymmetric configuration is still poorly investigated, especially when a strong guide field is present.

In a previous work, *Cazzola et al.* (2015) have shown that, during rapid island coalescence with no guide field, three different reconnection regions can be observed. These regions have been identified as X-regions, where similar traces as the traditional asymmetric X-point are observed, D-regions, where reconnection occurs between two diverging islands and reveals an opposite behavior with respect the X-regions, and M-regions, where the reconnection event occurs between two merging magnetic islands. In this work, a similar analysis leads to the identification of these three types of regions also in the case with guide field. It is important to identify parameters that allow high resolution satellites, such as the Magnetospheric MultiScale (MMS) NASA mission (*Burch et al.*, 2014), to distinguish between these three regions.

This work intends to give more insights into the electron behavior in these three specific regions, in support of future comparisons with observational data. Particular attention will be given to the departure of particles from the initial isotropy and gyrotopropy. In Particle-In-Cell (PIC) simulations, the departure from gyrotopropy is quantified from information collected in the pressure tensor. Several methodologies are available. Hereafter, we will refer to these methodologies as *detection algorithms* to underline their numerical nature based on a precise mathematical algorithm. The algorithms used in this work are those proposed by *Scudder and Daughton* (2008) ( $A\emptyset$ ), *Aunai et al.* (2013) ( $D_{ng}$ , shown in the supporting material) and *Swisdak* (2016) ( $\sqrt{Q}$ ). The first method focuses on particle agyrotropy in the plane perpendicular to the local magnetic field. It relies on the diagonalization of a pressure tensor specifically built upon the

perpendicular velocity direction, and easily retrievable from traditional PIC pressure tensors after some mathematical manipulation. The other two methods propose different algorithms which also include the parallel component in the computation. The mathematical formulation of these three metrics is summarized in the supporting material. None of these methods has been applied so far to the case of asymmetric island coalescence, either with or without guide field.

In addition to the previous quantities, we visualise electron agyrotropy by carrying out an analysis of the electron temperature in the frame of reference based on the local magnetic field. The parallel and the two orthogonal perpendicular directions to the local magnetic field  $T_{||}$ ,  $T_{\perp 1}$  and  $T_{\perp 2}$ , are identified according to the definition given in *Goldman et al.* (2015) and recalled in Section 2. The analysis of agyrotropy is addressed with the ratio  $T_{\perp 1}/T_{\perp 2}$ , while the ratio  $T_{||}/T_{\perp 1}$  is used to study the anisotropy.  $T_{\perp 1}/T_{\perp 2}$ , gives insight into *relative departure* from agyrotropy in the two direction  $\perp_1$  and  $\perp_2$ , which are not necessarily the directions where the temperature differs more. Notice the latter approach is strictly simulation-frame dependent, whereas quantities  $A\emptyset$ ,  $Q$  and  $D_{ng}$  instead address the perpendicular components independently of the simulation frame adopted. These quantities are computed from simulations results only, by not directly involving the simulation axis. A systematic comparison between the aforementioned metrics will be given to remark on their principal differences. Since the method proposed in *Aunai et al.* (2013) is conceptually similar to *Swisdak* (2016) (they both aim at highlighting non-gyrotropies in the 3D space) and gives similar results, it will be only shown in the supporting material.

In addition to the analysis, the electron velocity distributions for some particular region are given, including the X-, D- and M-regions

in order to reveal their characterizing signatures.

The paper is structured as follow. Section 2 gives further details on the simulation setup. Section 3 describes the most interesting results. Finally, the main conclusions are summarized in Section 4.

## 2 Simulation Setup

Results are shown for a set of 2.5D simulations performed with the fully kinetic massively parallel implicit moment method Particle-in-Cell code iPIC3D (Markidis *et al.*, 2010; Innocenti *et al.*, 2016). In 2.5D simulations all the vector quantities are three dimensional, but their spatial variation is assumed to be independent of the dawn-dusk ( $Z$ ) direction. A cartesian frame of reference is adopted, with the  $X$  coordinate parallel to the initial current sheet (North-South direction in GSM), the  $Y$  the direction parallel to the reversing  $B$  (Earth-Sun direction in GSM) and the  $Z$  the direction to complete the set accordingly (dawn-dusk direction in GSM). The simulated domain is a  $40 \times 40 d_i$  box with  $2048 \times 2048$  cells, where  $d_i = \frac{c}{\omega_{p,i}}$  is the ion skin depth referred to the magnetosheath conditions, to which all lengths in the code are normalized. The boundary conditions are periodic in all directions. The temporal step is  $\omega_{c,e} \cdot dt = 0.128$ , where  $\omega_{c,e}$  is the electron cyclo-frequency. The ion-electron mass ratio is  $m_i/m_e = 256$ . The plasma temperature across the layer is kept constant with an ion-electron temperature ratio  $T_i = 2T_e$ . The initial electron velocity is  $v_{th,e}/c = 0.1$ , and  $c/v_A = 113.6$ , where  $v_A$  is the Alfvén speed. The initial ion drift is neglected, and the initial current density is fully carried by electrons, as done in the literature (Pritchett, 2007). With the parameter here considered, we simulate a plasma with plasma beta  $\beta_{sh} \sim 1.2$  in the magnetosheath side and  $\beta_{sp} \sim 0.05$  in the magne-

sphere side. These values are compatible with those commonly observed in these regions, e.g.,  $\beta_{sh} \sim 2.4$  and  $\beta_{sp} \sim 0.27$  (Cassak and Fuselier, 2016). Two current sheets are configured at  $y_1 = \frac{1}{4}L_y = 10 d_i$  and  $y_2 = \frac{3}{4}L_y = 30 d_i$ , with a current sheet half-thickness  $L = 0.5 d_i$ . The magnetic field and density profiles across the current sheets are shown and described in the supporting material. We simulate two different current sheets to compare two different reconnection mechanisms.

The upper layer (i.e. the one centered at  $y_2 = 30 d_i$ ) is described by a continuous hyperbolic function (e.g. Quest and Coroniti, 1981; Pritchett, 2008; Pritchett and Mozer, 2009). An initial out-of-plane current density is initialized according to  $\nabla \times \mathbf{B}/\mu_0 = \mathbf{J}$ . An initial perturbation identical to that used in Lapenta *et al.* (2010) is set in the middle of the layer to produce a single X-point. In contrast, the lower layer (i.e. the one centered at  $y = 10 d_i$ ) is configured as a pure tangential discontinuity under an extremely steep gradient, with the same asymmetric profiles as the upper layer. No current density is initially set, causing this layer to be intrinsically highly unstable and suitable to gain more insights into physics of island coalescence in asymmetric reconnection. No initial perturbation is added to this layer. A strong current density is naturally formed during the very first stages of the simulation to counteract the initial imbalance. The same simulation is carried out with and without an initial guide field  $B_g = B_{0,x}$ .

## 3 Results

Figure 1 shows four different quantities in the two current sheets at  $\omega_{c,i} \cdot t \sim 21$ , for the case with no guide field (lefthand panels) and the case with guide field (righthand panels).

As already pointed out in Cazzola *et al.* (2015), at this time step the upper layer fea-

tures a typical asymmetric reconnection site (e.g. *Pritchett*, 2007, 2008; *Cassak and Shay*, 2007; *Swisdak et al.*, 2003). Meanwhile, the lower layer has rapidly evolved in the formation and growth of several magnetic islands, which in time progressively coalesce.

A first analysis is carried out in a frame of reference based upon the local magnetic field direction, as suggested in *Goldman et al.* (2015). The parallel and perpendicular directions are identified as follows

$$\begin{aligned}\hat{\mathbf{e}}_{\parallel} &: \mathbf{B} \times \hat{\mathbf{e}}_{\parallel} = 0 \\ \hat{\mathbf{e}}_{\perp 1} &= \mathbf{B} \times \hat{\mathbf{e}}_{\mathbf{z}} \\ \hat{\mathbf{e}}_{\perp 2} &= \mathbf{B} \times \hat{\mathbf{e}}_{\perp 1} = -\hat{\mathbf{e}}_{\mathbf{z}} B^2 + \mathbf{B} (\hat{\mathbf{e}}_{\mathbf{z}} \cdot \mathbf{B})\end{aligned}\quad (1)$$

Panels (a)-(h) in Figure 1 display the departure from the initial electron isotropy and gyrotropy by plotting the ratio between  $T_{\parallel}/T_{\perp 1}$  and  $T_{\perp 1}/T_{\perp 2}$  ( $T$  is the electron temperature). As  $T_{\parallel}/T_{\perp 1}$  and  $T_{\parallel}/T_{\perp 2}$  are very similar, the latter is not plotted here. The  $T_{\parallel}/T_{\perp 1}$  and  $T_{\perp 1}/T_{\perp 2}$  ratios give a quick information on the anisotropy and agyrotropy based on the simulation frame (notice the  $z$ -dependence in Eqs. 3). Quantities  $A\emptyset$  (*Scudder and Daughton* (2008), panels  $i - l$ ) and  $\sqrt{Q}$  (*Swisdak* (2016), panels  $m - p$ ) are instead computed to be independent of the simulation frame. As  $A\emptyset$  varies between 0 and 2, here the range is normalized to  $[0, 1]$  for a better comparison with the quantity  $\sqrt{Q}$ , which ranges  $[0, 1]$ .

One can see that some regions are highlighted in all the panels in the case without guide field, such as the upper separatrices in the single reconnection point, the lower separatrices in the lower current sheet and, to a lesser extent, the reconnection exhausts (i.e. at  $x \sim 14$  and  $y \sim 29.5$  d<sub>i</sub>) of the single X-point. These regions then show both anisotropic and agyrotropic behavior. Some other regions are instead only highlighted by  $T_{\parallel}/T_{\perp 1}$ ,  $A\emptyset$  and  $\sqrt{Q}$

and not seen in  $T_{\perp 1}/T_{\perp 2}$ , including: (1) the separatrices bordering the weaker field side, (2) the inflow region from the stronger field side (i.e.  $x \sim 20$ ,  $y \sim 30.5$  d<sub>i</sub>), and (3) the particular outflow observed between the islands near  $x \sim 37$  d<sub>i</sub> in the lower current sheet. The reason is that  $\hat{\mathbf{e}}_{\perp 1}$  is, by definition, in the simulation plane, but  $\hat{\mathbf{e}}_{\perp 2}$  is perpendicular to both  $\hat{\mathbf{e}}_{\perp 1}$  and  $\mathbf{B}$ . Hence, when  $\mathbf{B}$  is mostly in the plane (as it preferentially happens in the case without guide field as opposed to the case with guide field), the perpendicular to  $\mathbf{B}$  plane is nearly perpendicular to the simulation plane also.  $T_{\perp 1}/T_{\perp 2}$  shows the projection of temperature agyrotropy in the simulation plane. Thus, when  $B_g = 0$ ,  $T_{\perp 1}/T_{\perp 2}$  captures some, but not all, of the agyrotropic regions.  $A\emptyset$  and  $\sqrt{Q}$  do a better job. Notice also that  $A\emptyset$  and  $\sqrt{Q}$  are quite similar in the case without guide field.

Remarkable differences are identified in the case with guide field. The quantities  $A\emptyset$ ,  $\sqrt{Q}$  and  $T_{\perp 1}/T_{\perp 2}$  show a different agyrotropic behavior in some peculiar regions. Examples are at separatrices, which are highlighted both in  $T_{\perp 1}/T_{\perp 2}$  and  $A\emptyset$  plots, but very weakly displayed in  $\sqrt{Q}$ , and the area within the magnetic islands, which are more powerfully marked by the quantity  $\sqrt{Q}$  than  $A\emptyset$ . Given the importance of separatrices in magnetic reconnection (e.g. *Lapenta et al.*, 2015a,b), this difference is of fundamental importance for satellite observations. One can notice that the areas within the islands highlighted by  $\sqrt{Q}$  show a clear similarity with the anisotropy regions highlighted by  $T_{\parallel}/T_{\perp 1}$  (panels  $b$  and  $d$ ). This fact can be explained because in the formula for  $\sqrt{Q}$  the parallel pressure is accounted, while  $A\emptyset$  is constructed considering only the plane perpendicular to the local magnetic field. This is also the reason why the  $A\emptyset$  and  $T_{\perp 1}/T_{\perp 2}$  metrics show, in general, more similar results than  $\sqrt{Q}$ : in  $T_{\perp 1}/T_{\perp 2}$  and  $A\emptyset$  parallel pressure is not considered. Also, in the case with guide field, the  $\hat{\mathbf{e}}_{\perp 1} - \hat{\mathbf{e}}_{\perp 2}$  plane considered in  $T_{\perp 1}/T_{\perp 2}$

and the perpendicular plane used in  $A\mathcal{O}$  mostly superimpose.

Interesting is the analysis of the X-, D- and M-regions mentioned earlier, which can help distinguish the three regions during satellite observations. In *Cazzola et al.* (2015), X- and D-regions were identified by comparing the  $T_{\perp 1}/T_{\parallel}$  and  $T_{\perp 1}/T_{\perp 2}$  plots with the corresponding plots of the single X-point. M-regions were instead identified with the reconnection exhaust flowing out from an observed island merging. Here, a similar analysis is performed for the case with guide field. By observing panels (d) and (h), we notice that all the reconnection sites resemble the traces depicted in (b) and (f), with the only exception of the domain between  $x = 35$  and  $40 d_i$ , which shows an opposite behavior. The latter is typical of a D-region, so it can be identified accordingly. However, the upward-moving quadrupolar structure seen in the D-regions in *Cazzola et al.* (2015) and here visible in the case with no guide field (e.g. at  $x \sim 15 d_i$  in panel *g*) is no longer observed with guide field. Moreover, the agyrotropic structures seen in the plasmoid centers are also absent.

In light of the upcoming satellite observations, we show the electron phase-space for the domains marked with a black box in Figure 1. Two different sets of electron phase-spaces are shown in figure 2, respectively, for the case without guide field (panels *a1* - *n1*) and with guide field (panels *a2* - *n2*). Each box (which is not to scale for a clearer representation), represents a physical domain of  $0.12 \times 0.12 d_i$ , as a compromise between exact localization (which would require a smaller bin) and lack of noise in the representation. Notice that the same box number corresponds to comparable features in the case without and with guide field. Domains 1, 2 and 3 correspond to X-, D and M-regions for guide field values. Domain 4 represents the situation at the outflow of the M-regions. Domain 5 represents the situation at the separa-

trices. Finally, Domains 6 and 7 study the situation, respectively, in the O-point and the inner region within a magnetic island. Box numbers are replicated over all the plots for a better readability. To represent velocity we introduce the coordinate system  $\mathbf{V} = V_{\parallel} \hat{\mathbf{b}} + V_{\perp} \hat{\mathbf{\Omega}}$ , where  $\hat{\mathbf{b}}$  is the magnetic field direction and  $\hat{\mathbf{\Omega}}$  is the direction in the perpendicular plane. We plot the velocity distribution in the  $V_{\parallel} - V_{\perp}$  and  $V_{\perp} - \theta$  plane, where  $\theta \in [-\pi, \pi]$  is the angle between the direction  $\hat{\mathbf{e}}_1$  and  $V_{\perp}$  in the plane normal to  $\hat{\mathbf{b}}$ . Figure S2 in the supporting material gives a visual representation of how  $\theta$  is calculated and why it spans the  $[-\pi, \pi]$  range. Alongside these plots, we represent the phase-spaces in the same regions in the  $V_{\perp 1} - V_{\perp 2}$  plane for a direct comparison (panels ending with + in Figure 2). The color scale in Fig. 2 indicates the logarithm of the number of particles over the infinitesimal volume-velocity domain.

Regions of type X, Domains 1, show a very remarkable agyrotropy for both the case with no guide field (panel *b1*), and, less marked, with guide field (panel *b2*), as expected (*Hesse et al.*, 2016; *Chen et al.*, 2016). Additionally, in the case without guide field we notice the presence of a crescent-shape velocity distribution in the  $V_{\perp 1} - V_{\perp 2}$  plane (panel *b1+*). The same is not seen clearly in the case with guide field (panel *b2+*), although expected (*Hesse et al.*, 2016; *Chen et al.*, 2016; *Burch et al.*, 2016). This effect is probably due to the presence of a relatively strong guide field, which tends to dampening the particles agyrotropic behavior, by smearing out any possible crescent outcome. The latter also explains the lower agyrotropic rate observed in panel (b2) compared to the case without guide field in panel (b1).

Finally, the case with guide field shows a relevant particle anisotropy (panel *a2*), noticeable also from the  $T_{\parallel}/T_{\perp 1}$  plot. In the case with guide field, only the metric  $\sqrt{Q}$  shows a rele-

vant agyrotropy, mostly extended from the left outflow, whereas the trace in  $A\emptyset$  results very moderate. We explain this effect with the particle anisotropy in the computation of  $\sqrt{Q}$ .

The situation in the D-regions, Domains 2, are similar with and without guide field (panels *c1* - *c2* and *d1* - *d2*). The flat-top velocity distribution typical of these regions (Cazzola *et al.*, 2015) appears even more remarked in the case with guide field, associated with a strong anisotropy. The same agyrotropic features are detected in  $A\emptyset$  and  $\sqrt{Q}$ .

Interesting is the situation in the M-regions, i.e. Domains 3. The velocity distributions in panels (f1) and (f2) do not show any relevant agyrotropic features in neither case. The algorithms  $T_{\perp 1}/T_{\perp 2}$ ,  $A\emptyset$  and  $\sqrt{Q}$  for the case with no guide field also do not show any agyrotropy. However, the case with guide field is slightly different. While a null agyrotropy value is predicted by algorithms  $T_{\perp 1}/T_{\perp 2}$  and  $A\emptyset$ , quantity  $\sqrt{Q}$  instead indicates that a certain agyrotropy is present close to the merging point. We believe that this effect can be explained by the presence of a strong parallel component in the region, as confirmed by  $T_{\parallel}/T_{\perp 1}$ .  $\sqrt{Q}$  shows that the electron distribution is not isotropic. With the help of  $A\emptyset$  and the phase-spaces, we understand that the lack of isotropy is mostly driven by a strong anisotropy, which however does not exclude a moderate agyrotropy be present. Concerning the M-regions, we analyze their vertical reconnection outflow in Domains 4. In the case without guide field we observe all the quantities to highlight the presence of a strong agyrotropy, also confirmed by the corresponding phase-space (panel *h1*). In the case with guide field, a clear reconnection outflow is not seen, stressing the atypical behavior being held during the island merging in presence of a strong guide field.

We formerly mentioned that the main difference between  $A\emptyset$  and  $\sqrt{Q}$  lies in the case with guide field at the separatrices and within

the islands. The separatrix is studied in Domain 5, while Domains 6 and 7 focus on the situation within the magnetic islands. From panels (j1) and (j2) in Figure 2, we observe that, in the case without guide field, the separatrix shows a very moderate agyrotropy, similar to what pointed out by  $\sqrt{Q}$ . In the case with guide field, the agyrotropy is much better highlighted in panel (j2), which confirms what represented in  $T_{\perp 1}/T_{\perp 2}$  and  $A\emptyset$ . Conversely, the quantity  $\sqrt{Q}$  shows a much weaker agyrotropic signature in this region. Finally, the situation within the islands is analyzed in Domains 6 and 7. Domain 6 gives some insight into the island center, i.e. the O-point. In the case without guide field, signatures of agyrotropy are detected by  $T_{\perp 1}/T_{\perp 2}$  and  $A\emptyset$ , and less remarked in  $\sqrt{Q}$ . The phase-space analysis confirms the presence of agyrotropy mainly shown for mid-energy electrons (greenish band). Instead, in the case with guide field no agyrotropy is highlighted by either quantities, nor is by the corresponding phase-space (panel *l2*). This indicates that O-points in presence of a strong guide field show a different behavior compared to the traditional case without guide field. Finally, Domain 7 analyses the agyrotropic *patch* visible in the case without guide field and already pointed out in Cazzola *et al.* (2015). In the case with guide field, the same Domain gives information on the inner agyrotropic structure predominantly highlighted in  $\sqrt{Q}$ . From panels (n1) and (n2) we observe that an agyrotropic signature is present in the case without guide field, mostly confined for mid-energy electrons (yellowish band), while the case with guide field does not show any clear agyrotropy, showing however a remarkable anisotropy.

## 4 Conclusions

This work presents a systematic comparison of the electron agyrotropic behavior from PIC simulations of asymmetric magnetic reconnection during rapid island coalescence, with particular focus on the X-, D- and M-regions identified in *Cazzola et al.* (2015). Cases with and without guide field have been addressed. Three detection algorithms for highlighting agyrotropy have been compared: the ratio between the perpendicular temperature components, the method proposed in *Scudder and Daughton* (2008) and that in *Swisdak* (2016) (Fig. 1). Additionally, the ratio between the parallel and perpendicular components ( $T_{\parallel}/T_{\perp 1}$ ) is used to highlight anisotropic regions. Different regions have been analysed in terms of the electron velocity phase-space for a helpful comparison with observational data, including the X-, D- and M-regions pointed out in *Cazzola et al.* (2015) as well as other relevant regions. A new representation method is adopted here to better represent the relation between the velocity perpendicular components  $V_{\perp 1}$  and  $V_{\perp 2}$ . The phase-space in the same regions on the  $V_{\perp 1} - V_{\perp 2}$  plane are also plotted in Figure 2. Unlike the  $V_{\perp} - \theta$  representation, the latter seems less suited to highlighting agyrotropy features, except for the case in the X-regions, where important features are particularly detected.

Below we provide a summary description of the main findings for each region analysed, as well as a brief comment on the performance of the different algorithms compared. Additionally, Table 1 gives a wider and quicker summary of the features.

**Methodology Remarks** We observe that the ratios  $T_{\parallel}/T_{\perp 1}$  and  $T_{\perp 1}/T_{\perp 2}$  give a quick and reliable initial insight into the anisotropy and agyrotropy. However, these algorithms are simulation-frame dependent, unlike those

from such as *Scudder and Daughton* (2008) and *Swisdak* (2016).

A noticeable discrepancy is detected between the two metrics  $A\emptyset$  and  $\sqrt{Q}$  in some regions in the case with guide field. We observe that the detection of  $T_{\perp 1}/T_{\perp 2}$  is closer to  $A\emptyset$  than  $\sqrt{Q}$ . We interpret this difference as due to a strong relevance of the parallel component. The parallel component is not included in the computation of  $A\emptyset$ , while it enters the calculation of  $\sqrt{Q}$ . Since  $T_{\perp 1}/T_{\perp 2}$  does not consider the parallel component also,  $T_{\perp 1}/T_{\perp 2}$  and  $A\emptyset$  are tendentially similar. It is interesting to comment on how similar  $T_{\perp 1}/T_{\perp 2}$  and  $A\emptyset$  plots are in the case with and without guide field. In the case with guide field, the presence of a relevant parallel component in the out-of-plane direction makes the plane perpendicular to the magnetic field nearly parallel to the simulation plane. This fact leads the representation of  $T_{\perp 1}/T_{\perp 2}$  to be particularly similar to  $A\emptyset$ . In the case without guide field, the plane perpendicular to the local magnetic field can take different directions with respect to the simulation plane. Hence,  $T_{\perp 1}/T_{\perp 2}$  and  $A\emptyset$  are more different in the case without guide field.

We now focus on specific regions.

**Separatrices** The agyrotropy in the separatrices is differently represented in the case with guide field. Separatrices are weakly highlighted in  $\sqrt{Q}$  compared to  $A\emptyset$ . This is probably due to the parallel component accounted in the computation of  $\sqrt{Q}$ . The velocity distributions analysis confirmed the presence of a clear agyrotropic behavior along the separatrices in Domain 5 for the case with guide field (panels *j2* in Figure 2). However, the separatrix in Domain 5 in the case without guide field shows a very moderate agyrotropy (panel *j1*), in line with the prediction of  $\sqrt{Q}$ .

**X-Regions** These regions are present in both the cases with and without guide field. A relevant agyrotropy is observed in both the cases (panels *b1* and *b2*). The strong anisotropy drives a detection of non gyrotropy from the  $\sqrt{Q}$  metric.  $A\emptyset$  does not show agyrotropy (Fig. 1). Interestingly, the analysis of the phase-space on the  $V_{\perp 1} - V_{\perp 2}$  plane shows a crescent shape in the case without field. However, the same is not seen in the case with guide field, as instead expected (*Hesse et al.*, 2016; *Chen et al.*, 2016).

**D-Regions** Signatures of D-regions are observed also in the case with guide field. The agyrotropy in these regions is well represented by all the models. The velocity distributions additionally reveal agyrotropy in the cases with and without guide field (panel *d1* and *d2*). The first case shows a strong anisotropy and the typical flat-top velocity distribution pointed out in *Cazzola et al.* (2015) (Fig. 2, panels *c1* and *c2*).

**M-Regions and Outflow** M-regions are found in the cases with and without guide field. While the only noticeable agyrotropy is revealed by  $\sqrt{Q}$  for the case with guide field, velocity distributions show no presence of agyrotropy in either case. A remarked anisotropy is observed in these regions for the case with guide field. We attribute the signature in  $\sqrt{Q}$  to this latter. Domain 4 has been considered to analyse the reconnection outflow from the M-regions. In the case without guide field, a sharp agyrotropy trace is highlighted by all the quantities, and further confirmed by the corresponding phase-space (panel *h1*). The same Domain with guide field instead does not show any agyrotropy signature, neither from the detection algorithms nor from the phase-space.

**Magnetic Islands** The agyrotropic behavior within magnetic islands has been studied in Domains 6 and 7. In particular, Domains 6 represent the typical O-point. In the case without guide field,  $T_{\perp 1}/T_{\perp 2}$ ,  $A\emptyset$  and  $\sqrt{Q}$  all show an agyrotropic signature in the centre of the islands, even though with a different degree. This agyrotropy is confirmed by the velocity distribution in panel (11). The same Domain with guide field instead does not show any relevant agyrotropy, nor it does in the phase-space. This effect suggests that the O-points in the case with strong guide fields tend to behave differently than when a guide field is absent. Concerning the case with guide field, we observe important differences between  $A\emptyset$  and  $\sqrt{Q}$  within the islands: while  $A\emptyset$  detects a moderate agyrotropy only around specific closed magnetic field lines,  $\sqrt{Q}$  shows a more extended agyrotropic region within the islands (panels *l* and *p* in Fig. 1). Domains 7 intends to analyse this situation. In the case without guide field, it represents the situation at the agyrotropic *patch* already observed in *Cazzola et al.* (2015). The presence of agyrotropy is confirmed by all the algorithms, as well as the corresponding phase-space (panel *n1*). In the case with guide field, the corresponding phase-space shows that no relevant agyrotropy is present in this region.

## Acknowledgments

The present work is supported by the NASA MMS Grant NNX08AO84G. Additional support for the KULeuven team is provided by the European Commission DEEP-ER project, by the Onderzoekfonds KU Leuven (Research Fund KU Leuven) and by the Interuniversity Attraction Poles Programme of the Belgian Science Policy Office (IAP P7/08 CHARM). M.E.I. is funded by the FWO (Fonds Wetenschappelijk Onderzoek - Vlaanderen) postdoc-



toral fellowship reference 12O5215N. The simulations were conducted on the Pleiades supercomputer of the NASA Advanced Supercomputing Division (NAS), on the Discover supercomputer of the NASA Center for Climate Simulation (NCCS), on the computational resources provided by the PRACE Tier-0 framework and on the Flemish Supercomputing Center (VSC-VIC3). The data produced by the simulations are stored in HDF5 format on the NASA-NAS data servers.

## References

- Aunai, N., M. Hesse, and M. Kuznetsova (2013), Electron nongyrotropy in the context of collisionless magnetic reconnection, *Physics of Plasmas (1994-present)*, *20*(9), 092,903.
- Burch, J., T. Moore, R. Torbert, and B. Giles (2014), Magnetospheric multiscale overview and science objectives, *Space Science Reviews*, pp. 1–17.
- Burch, J., R. Torbert, T. Phan, L.-J. Chen, T. Moore, R. Ergun, J. Eastwood, D. Gershman, P. Cassak, M. Argall, et al. (2016), Electron-scale measurements of magnetic reconnection in space, *Science*, *352*(6290), aaf2939.
- Cassak, P., and S. Fuselier (2016), Reconnection at earths dayside magnetopause, in *Magnetic Reconnection*, pp. 213–276, Springer.
- Cassak, P., and M. Shay (2007), Scaling of asymmetric magnetic reconnection: General theory and collisional simulations, *Physics of Plasmas (1994-present)*, *14*(10), 102,114.
- Cazzola, E., M. E. Innocenti, S. Markidis, M. V. Goldman, D. L. Newman, and G. Lapenta (2015), On the electron dynamics during island coalescence in asymmetric magnetic reconnection, *Physics of Plasmas (1994-present)*, *22*(9), 092,901.
- Chen, L.-J., M. Hesse, S. Wang, N. Bessho, and W. Daughton (2016), Electron energization and structure of the diffusion region during asymmetric reconnection, *Geophysical Research Letters*, *43*(6), 2405–2412.
- Drake, J., M. Swisdak, H. Che, and M. Shay (2006), Electron acceleration from contracting magnetic islands during reconnection, *Nature*, *443*(7111), 553–556.
- Goldman, M., D. Newman, and G. Lapenta (2015), What can we learn about magnetotail reconnection from 2d pic harris-sheet simulations?, *Space Science Reviews*, pp. 1–38.
- Hesse, M., Y.-H. Liu, L.-J. Chen, N. Bessho, M. Kuznetsova, J. Birn, and J. L. Burch (2016), On the electron diffusion region in asymmetric reconnection with a guide magnetic field, *Geophysical Research Letters*, *43*(6), 2359–2364.
- Innocenti, M. E., A. Johnson, S. Markidis, J. Amaya, J. Deca, V. Olshevsky, and G. Lapenta (2016), Progress towards physics-based space weather forecasting with exascale computing, *Advances in Engineering Software*.
- Lapenta, G., S. Markidis, A. Divin, M. Goldman, and D. Newman (2010), Scales of guide field reconnection at the hydrogen mass ratio, *Physics of Plasmas (1994-present)*, *17*(8), 082,106.
- Lapenta, G., S. Markidis, A. Divin, D. Newman, and M. Goldman (2015a), Separatrices: The crux of reconnection, *Journal of Plasma Physics*, *81*(01), 325810,109.

- Lapenta, G., R. Wang, and E. Cazzola (2015b), Reconnection separatrix: simulations and observations, in *Magnetic Reconnection: Concepts and Applications*, edited by W. Gonzalez and E. Parker, Springer.
- Markidis, S., G. Lapenta, and R. Uddin (2010), Multi-scale simulations of plasma with ipic3d, *Mathematics and Computers in Simulation*, *80*(7), 1509–1519.
- Oka, M., T.-D. Phan, S. Krucker, M. Fujimoto, and I. Shinohara (2010), Electron acceleration by multi-island coalescence, *The Astrophysical Journal*, *714*(1), 915.
- Pritchett, P. (2007), Kinetic properties of magnetic merging in the coalescence process, *Physics of Plasmas (1994-present)*, *14*(5), 052,102.
- Pritchett, P. (2008), Collisionless magnetic reconnection in an asymmetric current sheet, *Journal of Geophysical Research: Space Physics (1978–2012)*, *113*(A6).
- Pritchett, P., and F. Mozer (2009), Asymmetric magnetic reconnection in the presence of a guide field, *Journal of Geophysical Research: Space Physics (1978–2012)*, *114*(A11).
- Quest, K. B., and F. V. Coroniti (1981), Tearing at the dayside magnetopause, *Journal of Geophysical Research: Space Physics (1978–2012)*, *86*(A5), 3289–3298.
- Scudder, J., and W. Daughton (2008), illuminating electron diffusion regions of collisionless magnetic reconnection using electron agyrotropy, *Journal of Geophysical Research: Space Physics (1978–2012)*, *113*(A6).
- Swisdak, M. (2016), Quantifying gyrotropy in magnetic reconnection, *Geophysical Research Letters*, *43*(1), 43–49, doi:10.1002/2015GL066980, 2015GL066980.
- Swisdak, M., B. Rogers, J. Drake, and M. Shay (2003), Diamagnetic suppression of component magnetic reconnection at the magnetopause, *Journal of Geophysical Research: Space Physics (1978–2012)*, *108*(A5).

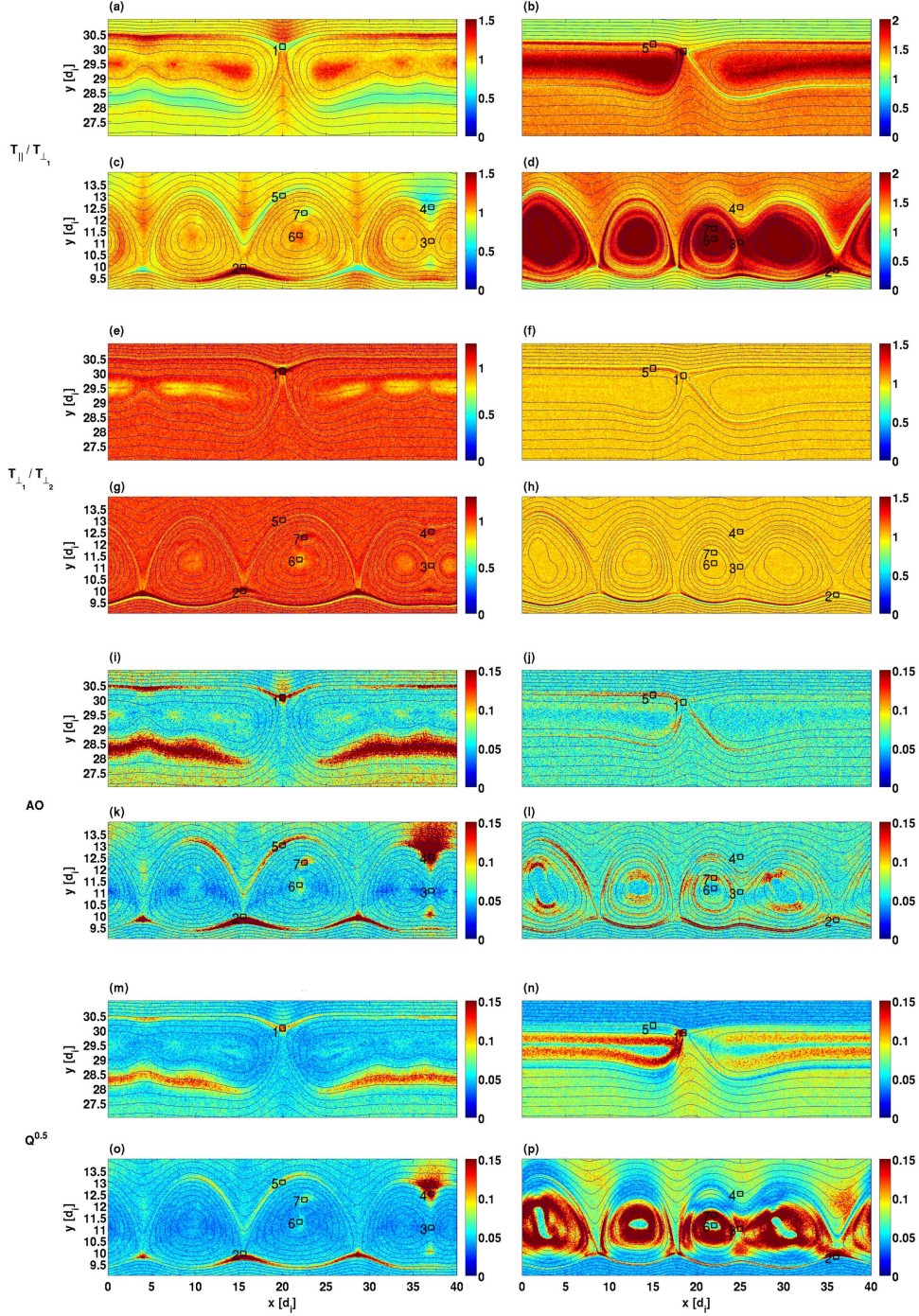


Figure 1: Plot of  $T_{\parallel}/T_{\perp 1}$ ,  $T_{\perp 1}/T_{\perp 2}$ ,  $A\phi$  and  $\sqrt{Q}$  for the two current sheets at  $t \sim 21 \omega_{ci}^{-1}$ , for the case with no guide field (left panels) and with guide field (right panels). Black boxes indicate the domains considered for the phase-spaces.

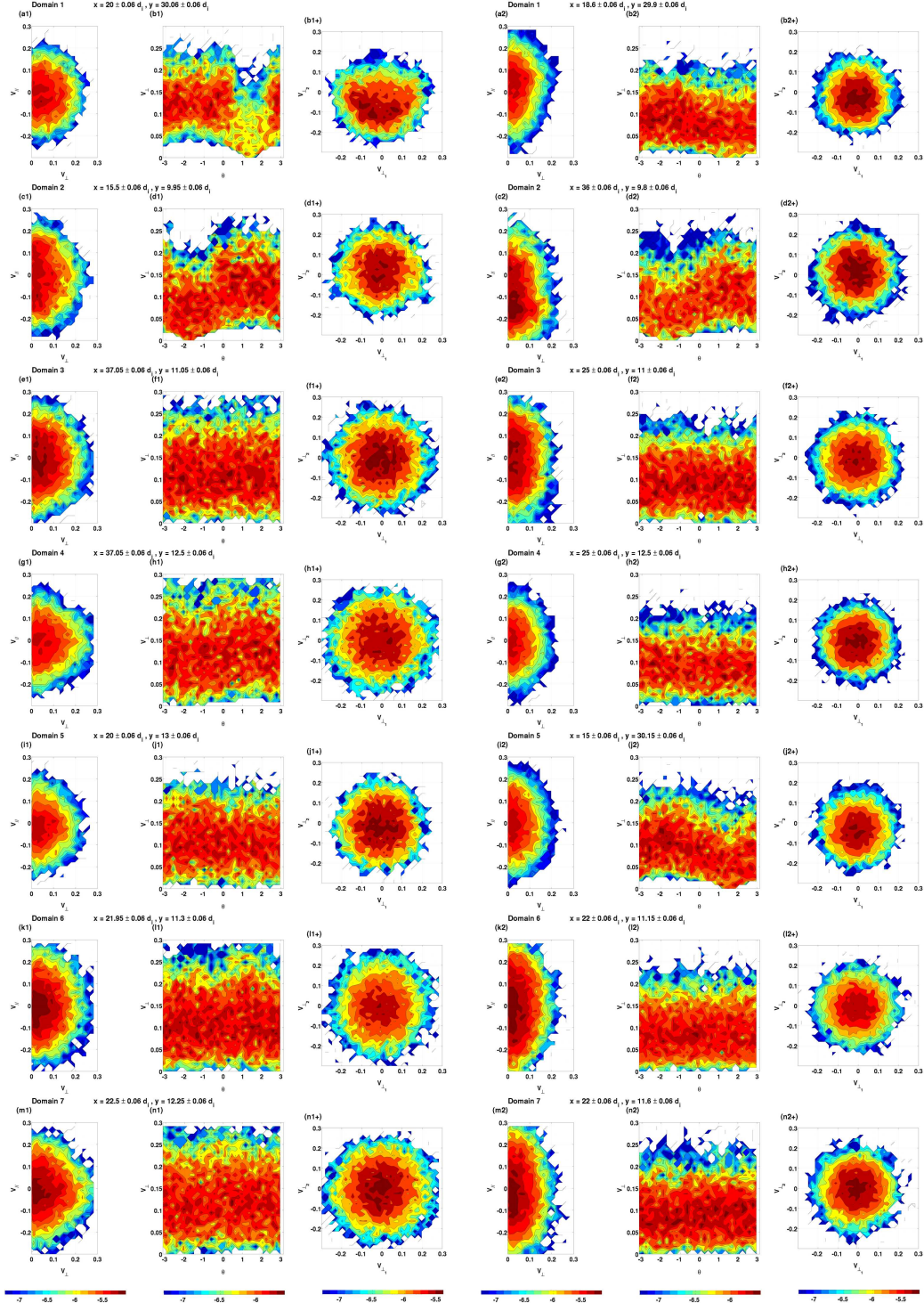


Figure 2: Set of electron velocity distributions for the domain pointed out with black boxes in figure 1. Color scale indicates the number of particles, in logarithmic scale, over the infinitesimal volume-velocity domain. Panels ending with 1 describe the case with no guide field, while those ending with 2 the case with guide field. Over the axis  $V_{\parallel}$ ,  $V_{\perp} = \sqrt{V^2 - V_{\parallel}^2}$  and  $\theta$  as explained in the text. Finally, panels ending with + represent phase-space in the  $V_{\perp 1} - V_{\perp 2}$  plane.



Table 1: Comparison Table among the different detection algorithms, including the velocity distribution analysis. Quantities  $T_{\parallel}/T_{\perp 1}$ ,  $T_{\perp 1}/T_{\perp 2}$ ,  $A\emptyset$  and  $\sqrt{Q}$  are described quantitatively as *Not-detected*, *Low*, *Medium* and *Remarked*.

Without Guide Field						
Region	$x_{\parallel}/T_{\perp 1}$	$T_{\perp 1}/T_{\perp 2}$	$A\emptyset$	$\sqrt{Q}$	$V_{\parallel} - V_{\perp}$	$\theta - V_{\perp}$
Method Features	Frame-dependent Useful for quick assessments Qualitative results Results similar to both $A\emptyset$ and $\sqrt{Q}$			Quantitative results $A\emptyset$ computed in the plane, $\sqrt{Q}$ computed 3D Strong agreement between the methods	Direct Comparison with Satellite observations Direct and Clear Assessment of anisotropy and agyrotropy	
	$T_{\parallel} < T_{\perp}$	$T_{\perp 1} > T_{\perp 2}$	15%	10 – 15%	low	Remarked Crescent-shape distribution on $V_{\perp 1} - V_{\perp 2}$ plane
Region D (Domain 2)	$T_{\parallel} > T_{\perp}$	$T_{\perp 1} > T_{\perp 2}$	15%	15%	Remarked double beam flat top distribution	Remarked
Region M (Domain 3)	$T_{\parallel} \sim T_{\perp}$	$T_{\perp 1} \sim T_{\perp 2}$	Not-detected	Not-detected	Low	Not-Detected
Region M - Outflow (Domain 4)	$T_{\parallel} < T_{\perp}$	$T_{\perp 1} \sim T_{\perp 2}$	15%	15%	Relevant for slow electrons	Medium
Separatrix (Domain 5)	$T_{\parallel} < T_{\perp}$	$T_{\perp 1} \sim T_{\perp 2}$	15%	10 – 15%	Relevant for slow electrons	Low
Magnetic Island Center - O-point (Domain 6)	$T_{\parallel} > T_{\perp}$	$T_{\perp 1} < T_{\perp 2}$	10%	5 – 10%	Low	Remarked for mid-energy electrons
Magnetic Island - Inner Patch (Domain 7)	$T_{\parallel} < T_{\perp}$	$T_{\perp 1} \sim T_{\perp 2}$	15%	5 – 10%	Low	Medium for mid-energy electrons
With Guide Field						
Region	$x_{\parallel}/T_{\perp 1}$	$T_{\perp 1}/T_{\perp 2}$	$A\emptyset$	$\sqrt{Q}$	$V_{\parallel} - V_{\perp}$	$\theta - V_{\perp}$
Method Features	Frame-dependent Useful for quick assessments Qualitative results Results similar to both $A\emptyset$ and $\sqrt{Q}$			Quantitative results $A\emptyset$ computed in the plane, $\sqrt{Q}$ computed 3D <i>Relevant disagreement</i> between the methods in some regions, such as separatrices	Direct Comparison with Satellite observations Direct and Clear Assessment of anisotropy and agyrotropy	
	$T_{\parallel} > T_{\perp}$	$T_{\perp 1} > T_{\perp 2}$	5%	15% only on one side	Low	Remarked
Region D (Domain 2)	$T_{\parallel} > T_{\perp}$	$T_{\perp 1} > T_{\perp 2}$	15%	15%	Strong double beam flat top distribution	Remarked
Region M (Domain 3)	$T_{\parallel} > T_{\perp}$	$T_{\perp 1} \sim T_{\perp 2}$	Not-detected	15%	Strong	Not-detected
Region M - Outflow (Domain 4)	$T_{\parallel} \sim T_{\perp}$	$T_{\perp 1} \sim T_{\perp 2}$	Not-detected	Not-detected	Low	Not-Detected
Separatrix (Domain 5)	$T_{\parallel} > T_{\perp}$	$T_{\perp 1} > T_{\perp 2}$	15%	Not-detected	Relevant for slow electrons	Medium
Magnetic Island Center - O-point (Domain 6)	$T_{\parallel} > T_{\perp}$	$T_{\perp 1} \sim T_{\perp 2}$	Not-detected	Not-detected	Remarked	Not-detected
Magnetic Island - Inner Closed Lines (Domain 7)	$T_{\parallel} > T_{\perp}$	$T_{\perp 1} \sim T_{\perp 2}$	$\sim 10\%$	15%	Remarked	Not-detected

# Supporting Information for "On the Electron Agyrotropy during Rapid Asymmetric Magnetic Island Coalescence in Presence of a Guide Field"

E. Cazzola<sup>\*1</sup>, M. E. Innocenti<sup>1</sup>, M. V. Goldman<sup>2</sup>, D. L. Newman<sup>2</sup>,  
D.S. Markidis<sup>3</sup>, and G. Lapenta<sup>1</sup>

<sup>1</sup>Department of Mathematics, KULeuven University, Celestijnenlaan  
200B, Leuven, 3001, Belgium.

<sup>2</sup>Center for Integrated Plasma Studies, University of Colorado  
Boulder, Boulder, Colorado, USA.

<sup>3</sup>PDC Center for high Performance Computing, KTH Royal Institute  
of Technology, Teknikringen 14, 10044 Stockholm, Sweden.

August 3, 2016

## Contents of this file

1. Figure S1
2. Figure S2
3. Figure S3

## Introduction

First of all, we report the magnetic field and density initial profiles adopted for the analysis

$$B_x(y) = \begin{cases} \frac{3}{2}B_0 & y \leq \frac{L_y}{4} \\ B_0 \left[ \tanh\left(\frac{y-y_2}{\lambda}\right) + R \right] & y > \frac{L_y}{4} \end{cases} \quad (1a)$$

$$y > \frac{L_y}{4} \quad (1b)$$

$$n(y) = \begin{cases} n_0(1-2\alpha) & y \leq \frac{L_y}{4} \\ n_0 \left[ 1 - \alpha \tanh\left(\frac{y-y_2}{\lambda}\right) \right] & y > \frac{L_y}{4} \\ -\alpha \tanh^2\left(\frac{y-y_2}{\lambda}\right) & \end{cases} \quad (2a)$$

$$y > \frac{L_y}{4} \quad (2b)$$

---

<sup>\*</sup>emanuele.cazzola@wis.kuleuven.be

where  $y_2 = \frac{3}{4}Ly$ ,  $\alpha = 0.33$  and  $R = 0.5$ , which lead to the profiles in Fig. 1.

In this supporting material section we include a more complete comparison of agyrotropy detection algorithms. In particular, we add the algorithm proposed in *Aunai et al.* (2013) (panels (q) through (t) in Fig. 2). Figure 2 shows the agyrotropic regions as computed from the algorithms proposed in *Scudder and Daughton* (2008) ( $A\emptyset$ ), *Swisdak* (2016) ( $\sqrt{Q}$ ) and *Aunai et al.* (2013) ( $D_{ng}$ ). The mathematical formulation of these three metrics is

$$\begin{aligned} A\emptyset &= 2 \frac{|\lambda_3 - \lambda_2|}{\lambda_3 + \lambda_2} \\ D_{ng} &= \frac{\sqrt{8(P_{xy}^2 + P_{xz}^2 + P_{yz}^2)}}{P_{||} + 2P_{\perp}} \\ Q &= 1 - \frac{4I_2}{(I_1 - P_{||})(I_1 + 3P_{||})} \end{aligned} \quad (3)$$

where  $\lambda_{2,3}$  are the non-trivial eigenvalues from the diagonalization of the pressure tensor constructed from distribution function perpendicular to the local magnetic field (see *Scudder and Daughton* (2008) for further details),  $I_1 = P_{xx} + P_{yy} + P_{zz}$  and  $I_2 = P_{xx}P_{yy} + P_{xx}P_{zz} + P_{yy}P_{zz} - (P_{xy}P_{yx} + P_{xz}P_{zx} + P_{yz}P_{zy})$ , and  $P_{ij}$  is the  $(i, j)$ -th term of the pressure tensor. All the quantities have been normalized to their maxima, with the maximum value for  $D_{ng}$  set to  $\sqrt{8/3}$ , as pointed out in *Swisdak* (2016). As done in the manuscript, the cases with and without guide field (respectively, right panels and left panels) at the same time are compared ( $\omega_{c,i} \cdot t \sim 21$ ). as can be noticed, *Swisdak* (2016) and *Aunai et al.* (2013)'s algorithms show similar results. These metrics both consider a tridimensional rendering, by including the parallel component of the pressure tensor in the assessment. Some small differences are however still noticeable, for example the value of agyrotropy for different scale needed in the two cases: for the case without guide field  $D_{ng}$  is around half of  $\sqrt{Q}$ , whereas the situation is reversed in presence of a guide field, where  $D_{ng}$  is nearly double of  $\sqrt{Q}$ . This last fact highlights once more the importance of the parallel component in the pressure tensor, mostly in presence of a guide field, which strongly influence the parallel behavior of particles and needs to be taken into account. Finally, another important difference is noticeable at the separatrices, where the quantity  $D_{ng}$  is more marked than  $\sqrt{Q}$ .

Additionally, Figure 3 gives a geometrical representation of the coordinate system  $\mathbf{V} = V_{||}\hat{\mathbf{b}} + V_{\perp}\hat{\mathbf{\Omega}}$  considered to highlight agyrotropy and anisotropy in the phase-spaces in Figure 2 of the manuscript. In particular,  $\hat{\mathbf{b}}$  is the direction parallel to the local magnetic field,  $\hat{\mathbf{\Omega}}$  is the direction in the perpendicular plane,  $\theta \in [-\pi, \pi]$  and  $V_{\perp} = \sqrt{V^2 - V_{||}^2}$ .

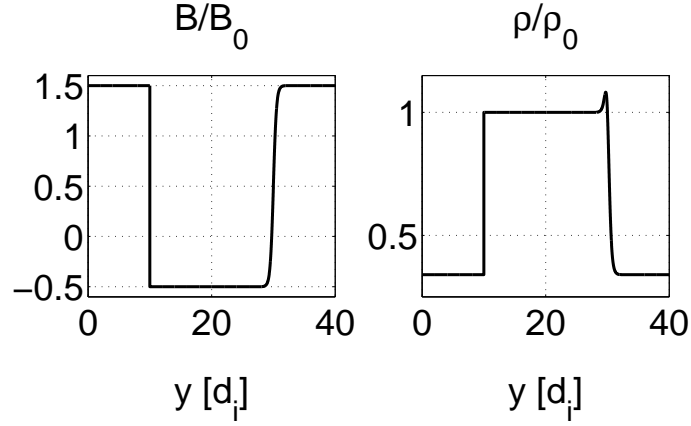


Figure 1: Initial profiles of magnetic field ( $B$ ) and density ( $\rho$ ) adopted. Notice how the periodicity is being respected at the boundaries.

## References

- Aunai, N., M. Hesse, and M. Kuznetsova (2013), Electron nongyrotropy in the context of collisionless magnetic reconnection, *Physics of Plasmas (1994-present)*, *20*(9), 092,903.
- Scudder, J., and W. Daughton (2008), illuminating electron diffusion regions of collisionless magnetic reconnection using electron agyrotropy, *Journal of Geophysical Research: Space Physics (1978–2012)*, *113*(A6).
- Swisdak, M. (2016), Quantifying gyrotropy in magnetic reconnection, *Geophysical Research Letters*, *43*(1), 43–49, doi:10.1002/2015GL066980, 2015GL066980.
- Swisdak, M., B. Rogers, J. Drake, and M. Shay (2003), Diamagnetic suppression of component magnetic reconnection at the magnetopause, *Journal of Geophysical Research: Space Physics (1978–2012)*, *108*(A5).



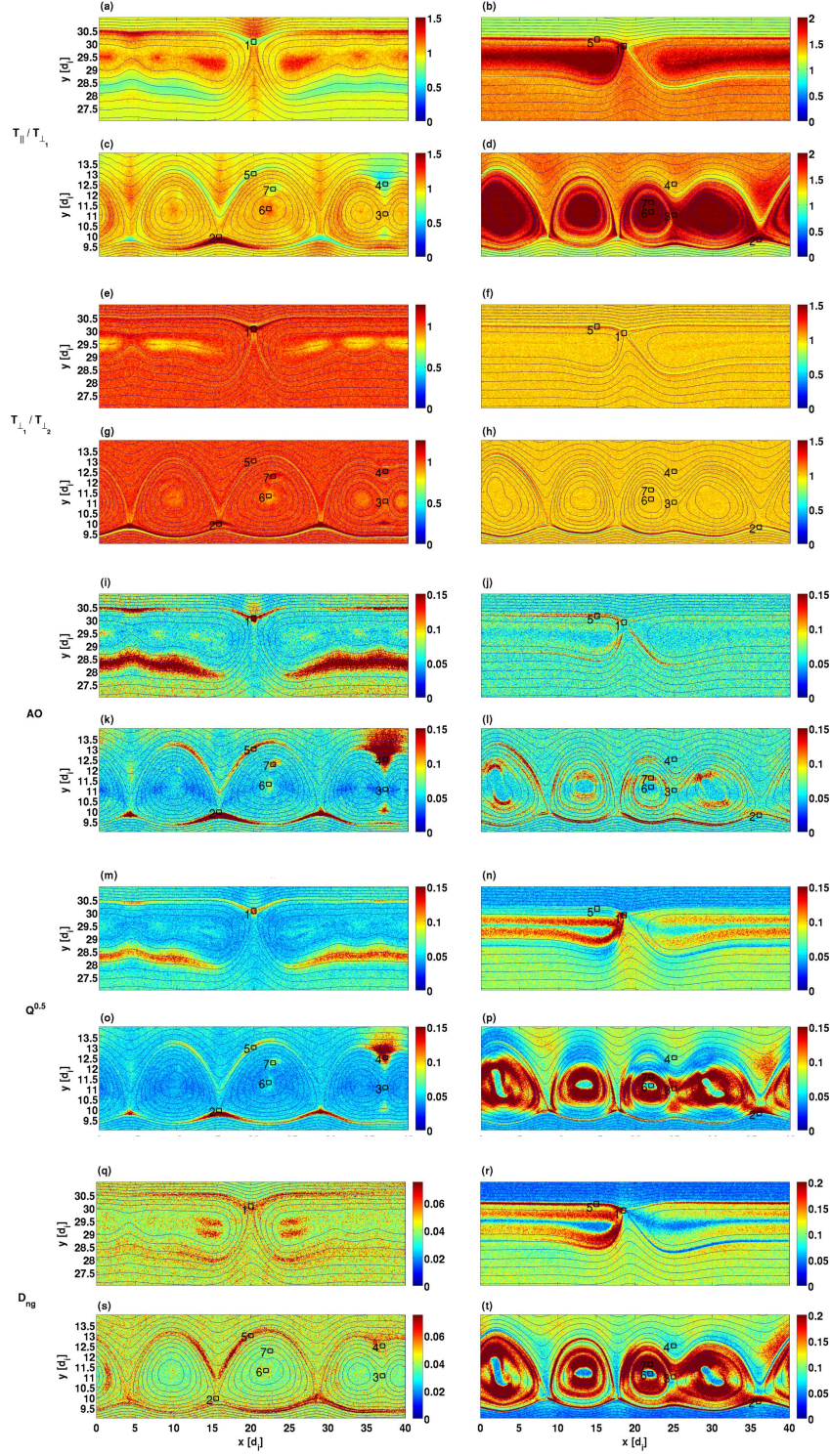


Figure 2: Plot of the agyrotropy detection algorithms proposed in (Scudder and Daughton, 2008) ( $AO$ ), (Swisdak et al., 2003) ( $\sqrt{Q}$ ) and Aunai et al. (2013) ( $D_{ng}$ ) for the two current sheets at  $t \sim 21 \omega_{ci}^{-1}$ , for the case with no guide field (left panels) and with guide field (right panels). Black boxes indicate the domains considered for the phase-spaces shown in the manuscript. All the quantities are normalized to the respective maxima. Refer to the text for further information.

